ROMANIAN JOURNAL OF INFORMATION SCIENCE AND TECHNOLOGY
Volume **18**, Number 1, 2015, 93–105

Nanostructured Titanium Doped Iron Oxide Photoelectrodes for Water Splitting

Cornel MICLEA[1], Luminiţa AMARANDE[1],
Marius Cristian CIOANGHER[1], Ciprian Tiberiu MICLEA[2,3],
Mădălina MIHĂILESCU[2], Cristina RADU[4], Anişoara IVANOV[5]

[1]National Institute for Materials Physics, Bucharest-Măgurele, Romania
[2]Hyperion University, Faculty of Physics, Bucharest, Romania
[3]University of Bucharest, Faculty of Physics, Bucharest-Măgurele, Romania
[4]Technical University for Civil Engineering, Bucharest, Romania
[5]Theoretical High School "Grigore Moisil", Tulcea, Romania

Corresponding author: cmic@infim.ro

Abstract. Water splitting by means of semiconducting photoelectrodes and solar light represents a promising alternative to conventional fossil fuel economy. In this process the photoactive electrode absorb sunlight directly thus initiating the photochemical reaction which create excess electrons in the conduction band of the semiconducting electrode. Titanium doped iron oxide seems to be a promising semiconducting material for photoelectrodes. Consequently, we investigated the effect of Ti doping on the structure, electrical and photoelectrochemical properties α-Fe_2O_3. The Ti doped α-Fe_2O_3 were prepared by a slightly modified mixed oxide route, consisting in a prolonged mixing of the raw materials in a high energy planetary ball mill until the particles decreased to the nanometric sizes. Optimum results were obtained for samples doped with 5 at. % titanium and sintered at 1200°C. Photocurrents as high as 8.4 mA/cm^2, for illumination from a 300 W xenon lamp, were recorded for such samples. It is hoped that such photoelectrodes show promise for water splitting.

1. Introduction

The Sun represents the most important source of energy for our life and therefore harvesting the solar energy attracted the attention of scientists, economists and even politicians. Besides the progress made in the art and science of photovoltaics [1-5], where the sunlight is directly converted into electrical energy, there is an alternative

method of collecting the solar energy and convert it into chemical energy that can be easily stored. This is the water splitting to give H_2 and O_2 by means of photoelectrochemical cells (PEC), which use a photoactive semiconducting electrode that can absorb sunlight and stimulate photochemical reactions by creating excess electrons in the conduction band, thus leading to the generation of hydrogen [6-8]. In this way the water splitting by PEC becomes one of the most promising means of producing hydrogen from a renewable source, a process that simple involves the breaking of water molecules into hydrogen and oxygen using sunlight. The most important class of materials, largely investigated as semiconducting photoelectrodes in PEC cells, is undoped and doped oxides of transition metals [9-11]. The first reported semiconductor electrode was the well known TiO_2, successfully used by Fujishima and Honda for water splitting some thirty years ago [12]. Since then the scientific and engineering interests in semiconductor photoelectrodes have significantly grown up and many studies have been devoted to this subject [13-25]. Though titania based photocatalysts proved to be good enough for hydrogen production by water splitting [7, 13, 25], the search for other more efficient photoelectrodes continues. A promising material that can possible replace titania is iron oxide, α-Fe_2O_3, which fulfills most of the requirements of a good photocatalyst. This oxide is the most abundant transition metal oxide on our planet, has desired electrical and chemical properties, is nontoxic, cheap and, most of all, has a lower band gap of only 2.2 eV as n-type semiconductor [26-33]. The conversion efficiency for hematite is relatively low due to its low light absorption and the high rate of electron-hole recombination. Therefore, it was suggested that conversion efficiency of hematite could be increased by doping with different ions as Mg, Zn, Si, Nb, W, Ta, Ge and some others [30, 33, 35-41]. It was thus reported an enhancement of about 65 % of the photocurrent density of silicon doped α-Fe_2O_3 for which a current density of 2.2 mA/cm^2 at 1.23 V_{RHE} was recorded [31]. Much higher densities of 3.7 mA/cm^2 were reported by Khan and Akikusa on nFe_2O_3 films at 0.7 V bias [27]. Values as high as 4 to 6 mA/cm^2 were reported by Sartoretti et al. [34] in their report on 2002, obtained on Ti 5 % doped αFe_2O_3 photoelectrodes.

In pure stoichiometric state the resistivity at room temperature of α-Fe_2O_3 is estimated at about 10^{14} ohm·cm, but small additions of different dopants or reducing some of the Fe^{3+} to Fe^{2+} state drastically decreases the resistivity, turning α-Fe_2O_3 into a n-type semiconductor with promising photocatalytic properties.

In the present investigation, we have studied the structure and photocatalytic properties of Ti doped α-Fe_2O_3 ceramic electrodes. Doping levels up to 10 at. % were used and the effect of doping proved to be important.

2. Experimental procedure

The compositions investigated consisted of iron oxide doped with Ti, corresponding to the formula: $Fe_{2-x}Ti_xO_3$, with x ranging from 0 to 0.1. The raw materials used for the sample preparation were a commercially available titania TiO_2 of 99.5 purity (Merck) and a high purity iron oxide α-Fe_2O_3 of 99.9 % purity (Johnson Matthey). The preparation method was a slightly modified mixed oxide route consisting in the

following: the stoichiometric amounts of oxides for each composition were mixed together, in hardened steel jars of 250 ml capacity using hardened steel balls of 10 and 15 mm diameter, in a high energy planetary ball mill type RETSCH PM 400, for up to 20 hours, in order to obtain a nanometric, more reactive powder with a uniform morphology and to allow a homogeneous distribution of the titanium into the iron oxide matrix. The ball/oxides weigh ratio for each composition was 5/1. The milling efficiency of material when using such a planetary ball mill is due to the fact that the grinding jars rotate around their own axis in opposite direction to the rotation direction of the main mill wheel at a ratio of 1/-2, meaning that they rotate twice for a single rotation of the main wheel. The rotation speed of the main wheel was set at 350 min^{-1}. The centrifugal forces combined with the Coriolis forces acting on the balls result in great frictional and impact forces, which produce a high degree of pulverization of material up to the nanometric sizes. The evolution of the mixing and milling process was analyzed by X-ray diffraction and by electron microscopy. The milled powders were annealed at 700 ^oC for 3 hours in order to remove as much as possible the mechanical stresses, deformations and defects of the lattice induced during milling. Disc shaped samples of 10 mm diameter and 1 mm thickness were then uniaxially pressed from this powders at a pressure of about 50 MPa using as binder only distilled water (about 5 % wt.) sprayed over the powder before pressing. The samples thus prepared were sintered at temperatures between 900 and 1350°C for 20 hours. The density of the sintered samples was determined by the Archimedes's method. The resistivity at room temperature was measured by the four points method applied directly on the disc metalised surface. Ohmic contacts were made by pyrolitically spraying a thin film of tin oxide on the sample surfaces followed by brushing and burning a conducting silver paste (Demetron). The photoelectrochemical properties were determined by means of a simple photoeletrochemical cell (PEC), specially designed for such measurements. It has a working electrode, a reference electrode and a counter electrode. The illumination source was a 300 W xenon lamp (Kratos model LH) maintained at a constant intensity of 50 mW/cm^2. The intensity of light was measured with a digital radiometer (model IL 1350) and a monocromator (Kratos model GM 100) was used to generate the light of a particular wavelength between 500 and 700 nm.

The photoelectrochemical performance was measured using a simple standard three electrode photoelectrochemical cell (PEC) fitted with a quartz window. The three electrodes were the working electrode (doped hematite), a platinum wire counter electrode and a reference electrode (standard calomel, SCE). The electrodes were immersed in 1 M NaOH electrolyte (pH=13.6). The samples were illuminated with a simulated sunlight provided by a 300 W xenon lamp (OSRAM) corresponding to a real light at AM 1.5G [41].

3. Results and discussion

Figure 1 shows an example of X-ray patterns for the mixed composition of iron oxide containing 5 % Ti, i. e. for the sample which could correspond to a formula like

$Fe_{1.95}Ti_{0.05}O_3$: The patterns for unmilled mixture (0 hours) exhibit clearly the peaks for both Fe_2O_3 (F) and TiO_2 (T) respectively, the more intense being the F ones.

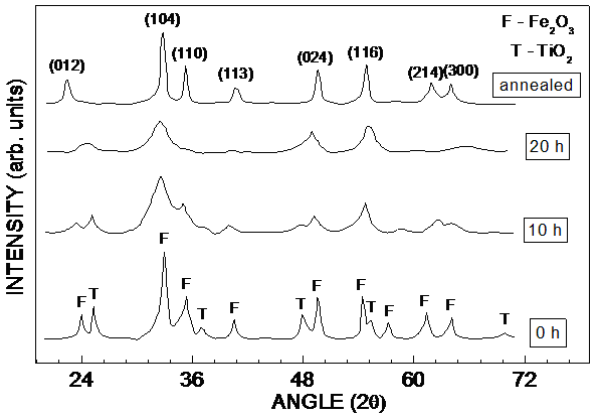

Fig. 1. X-ray patterns for a Ti doped sample milled for different times up to 20 hours.

After 10 hours of milling the T peaks decreases and some others start to vanish. After 20 hours of milling the T peaks completely disappear and the remaining ones are not clearly defined, due to the multitude of crystalline defects, induced into the lattice. A thermal annealing of this milled powder at 700°C for 3 hours removed to a great extent these defects and the peaks become more intense and well defined. No T peaks was found in this powder, which could be an indication that titanium atoms were uniformly incorporated into the Fe_2O_3 lattice and there is no separate region of TiO_2. It is like all TiO_2 particles "dissolved" into the Fe_2O_3 matrix. This allows to assume that nanometric sized titania particles distributed at first at the surface of the iron oxide particles were "swallowed" during milling into the Fe_2O_3 lattice, so that the titanium atoms have to be located at iron sites, this effect being facilitated by the high impact energy released during milling and by the similar ionic radia of Ti (0.68 Å) and Fe (0.64 Å). Figure 2 shows the morphology of the milled and annealed powder after 20 hours of milling. One can see that the particle size distribution is rather uniform and the particles shape is well defined. The average grain size was estimated to about 80 nm so that the milled powder is within the nanometric range.

The decrease of the particle size during milling is illustrated in Fig. 3 for the sample doped with 5 % titania. It is interesting to note the different rates of change of the particle size. Thus, for instance, in the first 5 hours the rate of change is more that 200 nm/hour while between 5 and 20 hours it decreased to less than 15 nm/hour and these rates show a constant behavior.

The densification process of the samples as a function of the sintering temperature is illustrated in Fig. 4 for three main compositions. One can see that the density for each composition increases nearly linearly with increasing sintering temperature up to a certain temperature, which in our case is situated around 1200°C, where it reaches a

maximum after which a slight decrease was observed due probably to a slight increases of the crystallite sizes together with the increase of some pores at the boundary grains.

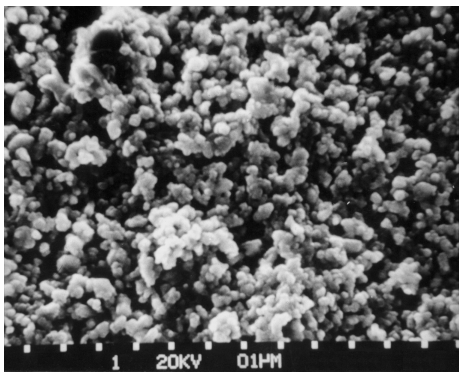

Fig. 2. SEM micrograph showing the morphology of Ti doped Fe_2O_3 powder sample after milled for 20 hours and annealed at 700°C for 3 hours.

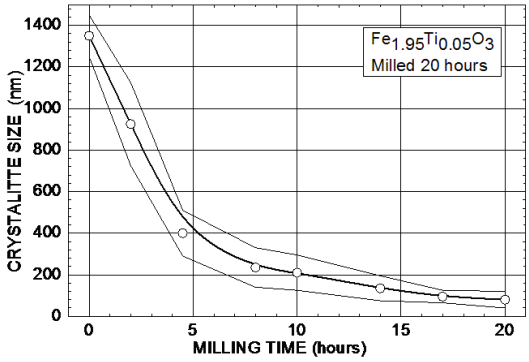

Fig. 3. The dependence of the powder crystallite size on the milling time.

With increasing the doping content, the density decreased as can be seen in Fig. 5 where the maximum density for each composition sintered at 1200°C is plotted as a function of composition. The decrease is nearly linear suggesting that probably the Ti atoms incorporate into the iron oxide lattice. These process could possible give rise to a slightly deformation of the lattice. The structure of the sintered samples at the optimum temperature is shown in the SEM image from Fig. 6, for the composition doped with 5 % titanium.

One may observe that the sample is rather well densified and the crystallite size, on average, is less than 1 μm. In addition there are no foreign phases segregated within the grains or at the grain boundaries thus confirming the supposition that titanium atoms incorporate into the lattice.

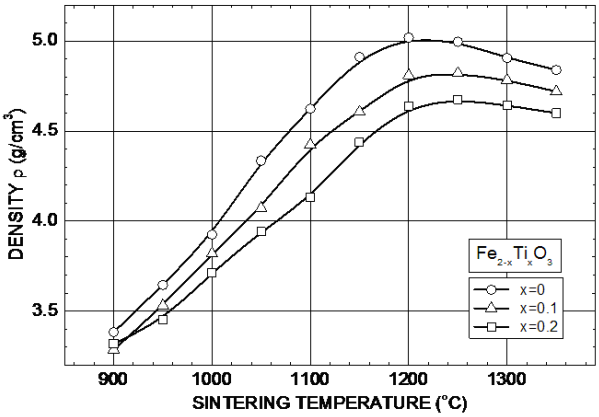

Fig. 4. The density vs. sintering temperature for some $Fe_{2-x}Ti_xO_3$ samples.

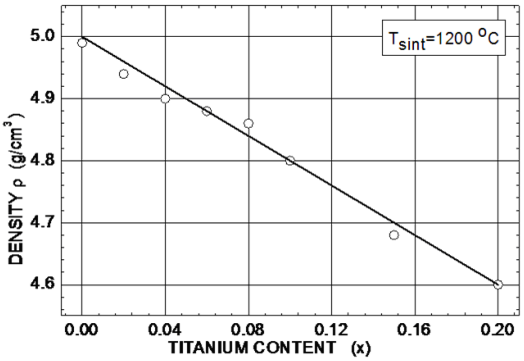

Fig. 5. The density vs. titanium content in $Fe_{2-x}Ti_xO_3$ samples sintered at 1200°C.

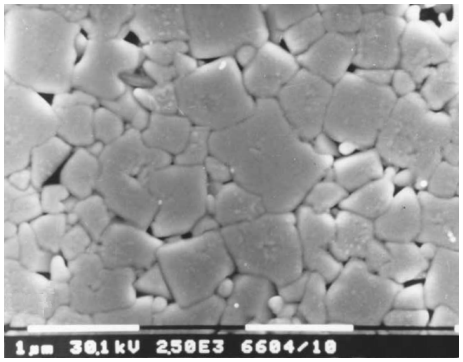

Fig. 6. SEM image of the structure of the $Fe_{1.95}Ti_{0.05}O_3$ sample sintered at 1200°C.

The electrical properties at room temperature were determined on sintered samples, mechanically processed as discs with plane parallel faces on which ohmic contacts were applied. The resistivity as a function of the Ti doping content is shown in Fig. 7 for all composition sintered at 1200°C.

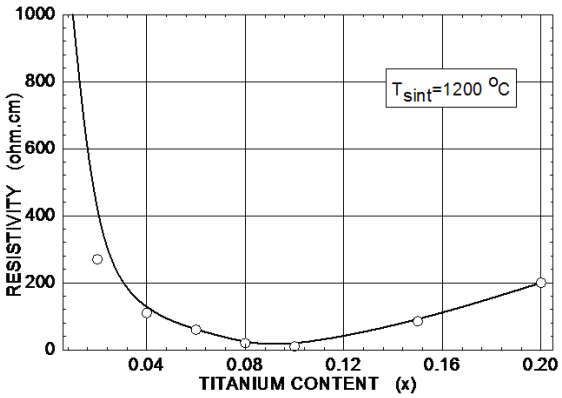

Fig. 7. The dependence of the room temperature resistivity of Ti doped Fe_2O_3 sintered samples.

For undoped samples the resistivity was around 10^7 ohm·cm suggesting either the presence of some undetected impurities in the raw hematite or that even at the sintering temperature of 1200°C some of the Fe^{3+} ions were reduced to Fe^{2+} state, thus creating some oxygen vacancies into the Fe_2O_3 that promote the n-type conduction. The resistivity drastically decreased by introducing the dopant until a minimum resistivity value of less than 20 ohm·cm for a doping level of 5 % Ti. The conduction mechanism in this case is due to Ti^{4+} ions which introduce electrons into the conduction band of Fe_2O_3, behaving now like a mixed valence compound with higher conductivity in which the conduction took place by hopping of electrons between Fe^{2+} and Fe^{3+} ions [26]. Going further with doping up to 10 % titanium, a slight increase of the resistivity up to 200 ohm·cm was observed, so that one may say that there is an optimum doping level around 5 % Ti where the conduction reaches the maximum value, thus expecting higher photocurrents.

The photoactivity of the electrodes was estimated by measuring the photocurrent density in the three electrodes photoelectrochemical cell with 1M NaOH as electrolyte at pH=13.6. The dependence of the photocurrent density as a function of measured electrode potential vs. SCE for some compositions prepared at optimum conditions is shown in Fig. 8. All samples show maximum values of the photocurrent density at 0.8 V. The photocurrent increases with increasing doping level reaching the highest value of 8.4 mA/cm^2 for composition containing 5 % Ti that is for sample with a composition, which could correspond to $Fe_{1.95}Ti_{0.05}O_3$.

This value of the photocurent we obtained on our Ti doped Fe_2O_3 represent about half of the theoretical maximum photocurrent for Fe_2O_3 as reported very recently in an excellent review paper by Z. Chen et al [42]. Such high values, up to 9-10 mA/cm^2, were also reported earlier by Strasik [26] for iron oxide photoelectrode doped with

0.1 % Si + 5% Pt, prepared by a freeze-drying process, claiming a much better homogeneity of the sample comparing with those obtained by conventional method.

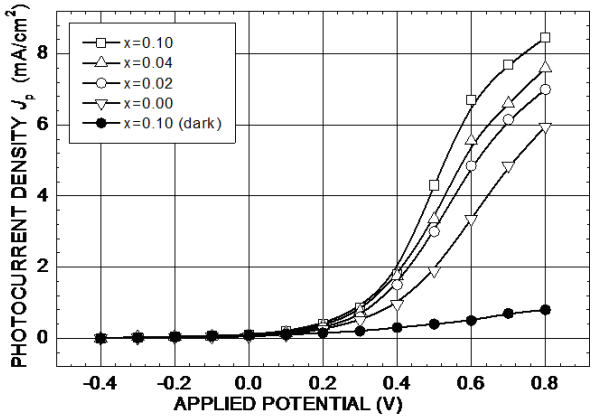

Fig. 8. The photocurrent density vs. electrode potential of SCE for some composition of $Fe_{2-x}Ti_xO_3$ sintered at 1200°C. The composition doped with 5 % Ti gave the highest current density of 8.4 mA/cm^2 at a potential of 0.8 V.

Consequently, we believe that the high value of the photocurrent we recorded could be an indication that our samples are also very homogeneous as well. Higher values of the photocurrent were also reported by Sartoretti et al. [34] (5 to 8 mA/cm^2 at 0.8 V_{SCE} for Ti doped α-Fe_2O_3 photoelectrodes in a structure with 2 to 3 electrodes in line. Khan and Akikusa [27] also obtained a current density of 3.7 mA/cm^2 at 0.7 V_{SCE} for n- Fe_2O_3 films synthesized by spray-pyrolisis method. A high value of 2.2 mA/cm^2 at 1.23 V_{RHE} was also reported by Kay et al[31] on Si doped α-Fe_2O_3 films at 1.23 V_{RHE} which was interpreted in terms of formation of an oriented dendritic nanostructure thus minimizing the distance the holes had to travel to the electrode/solution interface. Higher doping levels produce a decrease of the photocurrent as can be seen in Fig. 9 where the current density, at a bias voltage of 0.8 V, is plotted as a function of the doping level.

Optimum values for photocurrent were obtained for composition with a doping level around 5 % Ti. It is interesting to note that the difference between the photocurrent in darkness and that at illumination in the case of optimum conditions (5 % Ti doping and 0.8 V vs. SCE) is more than ten times greater (Fig. 8). Similar results were reported earlier [27] in the case of indium doped iron oxide thin films photoelectrodes. The dark current, though very low, exists and it slightly increases with increasing potential vs SCE and this could be possible explained by the direct tunneling across the space charge layer into the conduction band. In addition, it could also depend on the amount of defects and inhomogeneities along the grain boundaries where the charge transfer becomes possible.

In order to fully characterize the doped iron oxide photoelectrodes we also made capacitance and flat band potential measurements. It is known that flat band potential represents the potential at the electrode at which the semiconductor band is

flat it being a measure of the potential that must be applied to the semiconductor such that the bands remain flat when approaching the interface. It also determines the relative Fermi level of the semiconductor and electrolyte and the amount of band bending at the interface. Generally, the flat band potential V_{fb} can be determined by the Mott-Schottky capacitance method. The capacitance of the electrode is related to the electrode potential by the following relation:

$$1/C_{SC}^2 = \frac{2}{q\varepsilon\varepsilon_0 N_d}(V - V_{fb} - \frac{kT}{q}),$$

where C_{SC} is the capacitance per unit area of the space charge region, ε is the dielectric constant of the electrode, ε_0 is the permittivity of vacuum, q is the charge of the electron, N_d is the carrier density, $V$is the bias voltage at the electrode and V_{fb} the flat band potential. The slope of C_{SC}^{-2} vs V can provide the flat band potential. Figure 10 illustrates the Mott-Schottky plots for a number of compositions.

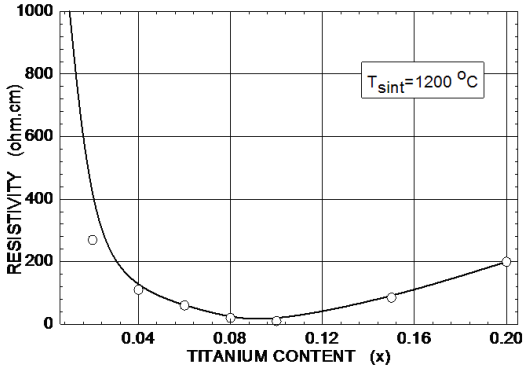

Fig. 9. The maximum photocurrent density vs. Ti concentration for $Fe_{2-x}Ti_xO_3$ photoelectrodes at a bias voltage of 0.8 V.

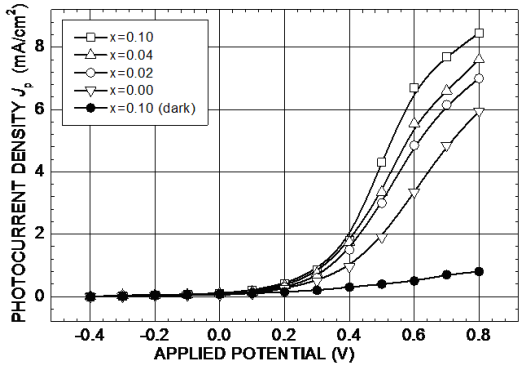

Fig. 10. Mott-Shottky plots of Ti-doped Fe_2O_3 photoelectrodes. The flat band potential was determined from the intersection of straight line with the bias voltage axis.

The plot is generally a straight line and the V_{fb} can be determined at the intersection of the extrapolating the linear portion of the data with the bias axis. The values of the flat band potential increases with increasing the doping level the tendency being to shift to positive values as can be noticed from Table 1.

It is thus probably that the flat band potential for heavily doped iron oxides to coincide with the band for majority carrier corresponding to the conduction band edge.

Table 1. The values of the flat band potential of the Ti doped Fe_2O_3 photoelectrodes as a function of compositions

Doping level x	Flat band potential V_{fb} (V)
0.00	– 1.15
0.02	– 1.01
0.04	– 1.02
0.06	– 0.98
0.08	– 0.11
0.10	– 1.02
0.15	– 0.50
0.20	– 0.78

4. Summary

Ceramic samples in the system $Fe_{2-x}Ti_xO_3$ were prepared by a slightly modified mixed oxide route and sintered at temperatures between 900 and 1350°C. Their structural, electrical and photoelectrochemical properties were investigated as a function of the doping level and processing parameters. The best materials were those with compositions situated around $Fe_{1.95}Ti_{0.05}O_3$ and sintered at 1200°C for which the basic parameters were at maximum. Such photoelectrodes are very promising to be used in photoelectrochemical cell for water splitting.

Acknowledgement. This work was partially supported by the NUCLEU Project of National Institute for Materials Physics, Măgurele. The authors acknowledge the financial support for making possible the dissemination of these results.

References

[1] SLAOUI A., COLLINS R., *Advanced materials for photovoltaics*, MRS Bull., **32**, pp. 211–218, 2007.

[2] MOMIRLAN M., VEZIROGLU T., *Renewable and sustainable energy*, Solar Energy, **74**, pp. 141–144, 2002.

[3] KODAMA T., *High temperature solar chemistry for converting solar heat to chemical fuels*, Progr. Energy Comb. Sci., **29**, pp. 567–597, 2003.

[4] SERPONE N., LAWLESS D., TERZIAN R., *Solar fuels; status and perspective*, Solar Energy, **49**, pp. 221-234, 1992.

[5] GOSWAMI D., VIJAYARAGHAVAN S., LU S., TAMM G., *New and emerging development in solar energy*, Solar Energy, **76**, pp. 33–43, 2004.

[6] BOLTON J.R., *Solar photoproduction of hydrogen. A Review*, Solar Energy, **57**, pp. 37–50, 1996.

[7] NI M., LEUNG M., LEUNG D., SUMATHY K., *A review of recent developments in photocatalytic water splitting for hydrogen production*, Renewable Sustainable Energy Review, **78**, pp. 1–26, 2005.

[8] KUDO A., *Development of photocatalytic materials for water splitting*, Int. J. Hydr. Energy, **31**, pp. 197–202, 2006.

[9] MORRISON S., *Electrochemistry at semiconductor and oxidized metal electrodes*, Ed. Plenum Press, New York, pp. 25–97, 1980.

[10] FINKELA H., *Semiconductor electrodes*, Ed. Elsevier, Amsterdam, pp. 147–202, 1988.

[11] GRANQUIST C., *Handbook of inorganic electrochemical materials*, Ed. Elsevier, Amsterdam, pp. 10–85, 1995.

[12] FUJISHIMA A., HONDA K., *Electrochemical photolysis of water at a semiconductor electrode*, Nature, **238**, pp. 37–38, 1972.

[13] FUJISHIMA A., RAO T., TRYK D.A., *Titanium dioxide photocatalyst*, J. Photochem. Photobiol C: Photochem. Rev., **1**, pp. 1–21, 2000.

[14] ZHOU Z., YE J., SAYAMA K., ARAKAWA H., *Direct splitting of water under visible light irradiation with an oxide semiconductor photocatalyst*, Nature, **414**, pp. 625–627, 2001.

[15] ASHOKKUMAR M., *An overview on semiconductor particulate systems for photoproduction of hydrogen*, Int. J. Hydrogen Energy, **23**, pp. 427–438, 1998.

[16] ASAHI R., MORIKAWA T., OHWAKI T., AOKI K., TAGA Y., *Visible light photocatalysis by Cu in nitrogen doped titanium oxide*, Science, **293**, pp. 269–271, 2001.

[17] LI X., LU X., LI S., *Photocatalytic production of hydrogen in single component and mixture systems of electron donors and monitoring adsorbtion of donors*, *Chemosphere*, **52**, pp. 843–850, 2003.

[18] ABE R., SAYAMA K., DOMEN K., ARAKAWA H., *A new type of water splitting system composed of two different TiO_2 photocatalysts (anatase-rutile) and IO_3^-/I^- redox mediator*, Chem.Phys. Lett., **344**, pp. 339–344, 2001.

[19] PAOLA A., MARCI G., PALMISANO L., SCHIAVELO M., UOSAKI K., IKEDA S., *Preparation of polycrystalline TiO_2 impregnated with various metal ions*, J. Phys. Chem. B, **106**, pp. 637–645, 2002.

[20] KOBAYAKAWA K., MURAKAMI K., SATO Y., *Visible light active N-doped TiO_2*, Int. J. Photochem. Photobiol A: Chem., **170**, pp. 177–179, 2004.

[21] TORRES G., LINDGREN T., LU J., GRANQUIST C., LINDQUIST S., *Photoelectrochemical study of N-doped TiO_2 for water oxidation*, J. Phys. Chem. B, **108**, pp. 1546–1549, 2004.

[22] GOLE J., STOUT J., BURDA C., LOU Y., CHEN X., *Highly efficient formation of visible light tunable IV-doped TiO_2*, J. Phys. Chem. B, **108**, pp. 1230–1240, 2004.

[23] FOX M., DULAY M., *Heterogeneous photocatalysts*, Chem. Rev., **93**, pp. 341–357, 1993.

[24] MILLS A., HUNTE S., *An overview of semiconductor photocatalysts*, J. Photochem. Photobiol A: Chem., **108**, pp. 1–35, 1997.

[25] TRYK D.A., FUJISHIMA A., HONDA K., *Recent topics in photoelectrochemistry: achievements and future prospects*, Electrochim. Acta, **45**, pp. 2363–2376, 2000.

[26] STRASIK M., *Photoelectrochemical and photocatalytic investigation of semiconducting iron oxide*, PhD Thesis, 1988.

[27] KHAN S.U.M., AKIKUSA J., *Photoelectrochemical splitting of water at nanocrystalline n-Fe_2O_3 thin films*, J. Phys. Chem. B, **103**, pp. 7184–7189, 1999.

[28] YARAHMADI S.S., WIJAYANTHA K.G.U., TAHIR A.A., VAIDHYANATHAN B., *Nanostructured α-Fe_2O_3 electrodes for solar driven water splitting: effect of doping agents on preparation and performance*, J. Phys. Chem. C, **113**, pp. 4768–4778, 2009.

[29] DURET A., GRATZEL M., *Visible Light-Induced Water Oxidation on Mesoscopic a-Fe_2O_3 Films Made by Ultrasonic Spray Pyrolysis*, J. Phys. Chem. B, **109**, pp. 17184–17191, 2005.

[30] AROUTIOUNIAN V.M., ARAKELYAN V.M., SHAHNAZARYAN G.E., HOVHANNISYAN G.E., WANG H.R., TURNER J.A., *Photoelectrochemistry of tin-doped iron oxide electrodes*, Solar Energy, **81**, pp. 1369–1376, 2007.

[31] KAY A., CESAR I., GRATZEL M., *New Benchmark for Water Photooxidation by Nanostructured α-Fe_2O_3Films*, J. Am. Chem. Soc., **128**, pp. 15714–15721, 2006.

[32] CESAR I., KAY A., MARTINEZ J., GRATZEL M., *Translucent Thin Film Fe_2O_3 Photoanodes for Efficient Water Splitting by Sunlight: Nanostructure-Directing Effect of Si-Doping*, J. Am. Chem. Soc., **128**, pp. 4582–4583, 2006.

[33] GLASSCOCK J. A., BARNES P.R.F., PLUMB I.C., SAVVIDES N., *The enhancement of photoelectrochemical hydrogen production from hematite thin films by the introduction of Ti and Si*, J. Phys. Chem. C, **111**, pp. 16477–16488, 2007.

[34] SARTORETTI C.J., ULMANN M., ALEXANDER B.D., *La photolyse de l'eau et la production d'hydrogene au moyen de l'energy solair*, Rapport annuel 2002. Office federal de l'energie 3003 Berne, Switzerland. (*The photolysis of water and hydrogen producing using energy from the Sun*, Annual Report 2002. Federal Office of Energy 3003 Bern, Switzerland).

[35] YARAHMADI S.S., WIJAYANTHA K.G.M., TAHIR A.A., VAIDHYANATHAN B., *Nanostructured α-Fe_2O_3 electrodes for solar driven water splitting: Effect of doping agents on preparation and performance*, J. Phys. Chem. C, **113**, pp. 4768–4778, 2009.

[36] MCALPINE N.S., FREDLINE R.A., *Characterization of Ti-doped α-Fe_2O_3 electrodes by impedance measurements*, J. Electroanalytical Chem., **252**, pp. 61–69, 1988.

[37] INGLER W.B., KHAN S.U.M., *Photoresponse of spray pyrolitically synthesized Mg doped oxide (p-Fe_2O_3) thin films under solar simulated light illumination*, Thin Solid Films, **461**, pp. 301–308, 2004.

[38] INGLER W.B., BAETRUS J.P., KHAN S.U.M., *Photoresponse of p-type Zn doped iron oxide thin films*, J. Am. Chem. Soc., **126**, pp. 10238–10239, 2004.

[39] CESAR I., KAY A., GONZALES MARTINEZ J.A., GRATZEL M., *Translucent thin film Fe_2O_3 photoanodes for efficient water splitting by sunlight: Nanostructure directing effect of Si-doping*, J. Am. Chem. Soc., **128**, pp. 4582–4583, 2006.

[40] HU Y.S., KLEIMAN-SHWARSCTEIN A., STUCKY G.D., MCFARLAND E.W., *Improved photoelectrochemical performance of Ti-doped α-Fe_2O_3 thin films by surface modification with fluoride*, Chem. Commun., **21**, pp. 2652–2654, 2009.

[41] MULLEJEANS M., IOANNIDES A., KENNY R., ZAAIMAN W., OSSENBRINK H.A., DUNLOP E.D., *Spectral mismatch in calibration of photovoltaic reference device by global sunlight method*, Meas. Sci. Technol., **16**, pp. 1250–1255, 2005.

[42] CHEN Z., JARAMILLO T.F, DEUTSCH T.G., KLEIMAN-SHWARSCTEIN A., FORMAN A.F., GAILLARD N., GARLAND R., TAKANABE K., HESKE C., SUNKARA M., MCFARLAND E.W., DOMEN K., MULLER E.L., TURNER J.A., DINH H.N., *Accelerating materials development for photoelectrochemical hydrogen production: Standards for methods, definitions and reporting protocols*, J. Mater. Res., **25**, pp. 3–16, 2010.